IVYSPRING INTERNATIONAL PUBLISHER

*Theranostics*

2016; 6(4): 485-500. doi: 10.7150/thno.13411

Research Paper

# A Multimodal System with Synergistic Effects of Magneto-Mechanical, Photothermal, Photodynamic and Chemo Therapies of Cancer in Graphene-Quantum Dot-Coated Hollow Magnetic Nanospheres

Fangjie Wo[1], Rujiao Xu[1], Yuxiang Shao[1], Zheyu Zhang[1], Maoquan Chu[1]✉, Donglu Shi[1, 2], Shupeng Liu[3]

1. Research Center for Translational Medicine at Shanghai East Hospital, School of Life Sciences and Technology, Tongji University, Shanghai, PR China.
2. The Materials Science and Engineering Program, Dept of Mechanical and Materials Engineering, College of Engineering and Applied Science, University of Cincinnati, Cincinnati, 45221, USA.
3. Institute of Biomedical Engineering, Shanghai University, Shanghai 200444, P. R. China.

✉ Corresponding author: mqchu98@tongji.edu.cn



Received: 2015.07.31; Accepted: 2015.11.24; Published: 2016.02.13

## Abstract

In this study, a multimodal therapeutic system was shown to be much more lethal in cancer cell killing compared to a single means of nano therapy, be it photothermal or photodynamic. Hollow magnetic nanospheres (HMNSs) were designed and synthesized for the synergistic effects of both magneto-mechanical and photothermal cancer therapy. By these combined stimuli, the cancer cells were structurally and physically destroyed with the morphological characteristics distinctively different from those by other therapeutics. HMNSs were also coated with the silica shells and conjugated with carboxylated graphene quantum dots (GQDs) as a core-shell composite: HMNS/$SiO_2$/GQDs. The composite was further loaded with an anticancer drug doxorubicin (DOX) and stabilized with liposomes. The multimodal system was able to kill cancer cells with four different therapeutic mechanisms in a synergetic and multilateral fashion, namely, the magnetic field-mediated mechanical stimulation, photothermal damage, photodynamic toxicity, and chemotherapy. The unique nanocomposites with combined mechanical, chemo, and physical effects will provide an alternative strategy for highly improved cancer therapy efficiency.

Key words: Drug-loaded magnetic nanocomposites; graphene quantum dots; magnetic field-mediated mechanical stimulation; near-infrared laser; cancer therapy.

## Introduction

Magnetic iron oxide $Fe_3O_4$ nanoparticles have consistently shown promise in biomedicine including drug delivery, magnetic resonance imaging contrast-enhancement agents, immunoassay, bioseparation, and magnetically induced hyperthermia therapy [1]. Various magnetic iron oxide nanoparticles have now been approved by the US Food and Drug Administration for clinical use [2].

The most common medical application of the magnetic nanoparticles has been hyperthermia via an alternating magnetic field (AMF). Magnetic hyperthermia treatment [3-6] is known for its low side effects compared to chemotherapy or radiotherapy [1]. However, magnetic hyperthermia has certain limitations in cancer treatment due to required high AMF currents and voltages [2].

In recent years, the use of magnetic particles for destruction of cancer cells using external mechanical forces transmitted by low-frequency AMF-induced vibrations has also attracted great attention [7–10]. In this method, the low-frequency AMF does not generate heat, but mechanical vibrations of the magnetic

particles. Novosad and coworkers [7] fabricated antibody-conjugated gold-coated ferromagnetic disks (~1 μm diameter, 60 nm thick; with a 5-nm-thick gold shell) and demonstrated cancer cell apoptosis by mechanical stimulation of the cell membrane using the biofunctionalized ferromagnetic disks under a magnetic field of 90 Oe at less than 60 Hz. Recently, Zhang et al. [9] conjugated the lysosomal-associated membrane protein 1 (LAMP1) antibody onto 100-nm-diameter superparamagnetic iron oxide nanoparticles (SPIONs) and incubated them with rat insulinoma cells. They found the lysosome membranes of the cells ruptured by the rotation of SPIONs. They also found the membrane permeability enhanced upon loading the LAMP1-SPION to cells while exposing to a magnetic field of ~30 mT. Shi and coworkers [10] developed the spherical (200±50 nm diameter) and rod-shaped (length: 200±50 nm, diameters: ~50–120 nm) $Fe_3O_4$ nanoparticles without antibody conjugation for effective cell killing under 35-kHz AMF. These previous works [7, 9, 10] showed negligible thermal insult to cells induced by AMF in their experiments.

More recently, cancer photothermal therapy using magnetic iron oxide nanoparticles [11–16] has also drawn great interest for its safe, convenient, and simple technique. For example, $Fe_3O_4$ nanoparticles could rapidly generate heat when exposed to near-infrared (NIR) laser irradiation, and the mouse tumor (grown from human esophagus carcinoma cells) growth was found to be significantly inhibited by the photothermal effect of these $Fe_3O_4$ nanoparticles [12].

However, in clinical practice, cancer may not be easily cured by using a single therapeutic means alone. Synergetic effects of multiple treatments often show much higher efficacy in cancer therapy. Therefore, in this study, we combined the functionalities of mechanical force and photothermal stimulation by using the hollow magnetic nanospheres (HMNSs) of $Fe_3O_4$. HMNSs were also coated with a silica shell containing amino groups for conjugation with carboxylated graphene quantum dots (GQDs) via an amino bond. The composites of HMNS/$SiO_2$/GQDs were then loaded with an anticancer drug doxorubicin hydrochloride (DOX). To improve the suspension stability of nanoparticles in aqueous solution, the HMNSs and their composites were dispersed with liposomes. Liposome exhibits excellent biocompatibility. This vesicle like lipid nanoparticle is one of the most important drug delivery systems used in clinical settings.

Although dual-modal and multimodal systems for cancer imaging and therapy have been reported by many research groups [14-16], the DOX-loaded HMNS/$SiO_2$/GQDs nanocomposites developed in this work are characterized by the following advantages: 1) high drug loading capacity; 2) efficient cancer cell killing by magnetic field-mediated mechanical force and chemotherapy; 3) photothermal, photodynamic, and chemotherapy in a synchronized fashion, and 4) the synergistic effects by four different mechanisms, namely, magnetic field-mediated mechanical stimulation, photothermal damage, photodynamic toxicity, and chemotherapy.

Localized treatments are convenient for esophageal cancer therapy. Therefore, photothermal and photodynamic therapy [12, 17, 18], hyperthermia [18] and radiotherapy [19] are often chosen for animal experiments and clinical treatment of esophageal cancer. We selected Eca-109 esophageal cancer cells in this study. The composites of HMNS/$SiO_2$/GQDs were used for in vitro experiments via NIR and magnetic field induced therapeutic means.

Figure 1 is the schematic diagram showing the formation of DOX-loaded magnetic nanospheres, stabilized with liposomes, and cancer cell killing by magnetic field-mediated mechanical force and NIR laser irradiation. The liposome-coated, DOX-loaded nanocomposites can provide multimodal therapy under an external magnetic field and NIR laser irradiation. The GQDs are selected for their sheet-like carbon-based structure, only 3–10 nm in size, that is ideal for a high drug-loading capacity [20]. In particular, they are capable of generating intracellular reactive oxygen species (ROS) upon NIR laser irradiation [21] for improving cell-killing efficiency. Furthermore, GQDs exhibit ultralow toxicity in vitro and in vivo [22]. The multifunctional nanocomposites utilizing both external magnetic field and NIR laser irradiation will have great potential in improving cancer therapy efficiency.

## 2. Materials and Methods

### 2.1. Chemicals and cell lines

The $FeCl_3 \cdot 6H_2O$, L-glutamic acid, soybean phospholipids, polyvinylpyrrolidone (PVP) K-30, tetraethyl orthosilicate (TEOS), (3-aminopropyl)triethoxysilane (APTES), DOX, N-Hydroxysuccinimide (NHS), $NH_4Ac$, ethylene glycol, chloroform, ethanol, and ammonium hydroxide were purchased from Sinopharm Chemical Reagent Co., Ltd. (Shanghai, China). The 1-Ethyl-3-(3-dimethylaminopropyl)-carbodiimide (EDC) was purchased from J&K (Atlanta, GA, USA). The RPMI-1640 culture medium and fetal calf serum (FCS) were obtained from Hyclone (Logan, UT, USA). The Hoechst 33342/propidium iodide (PI) double staining kit and 2,7-dichlorofluorescin diacetate (DCFH-DA) were provided by Beyotime Institute of Biotechnology

(Jiangsu, China). The CellTiter-Glo® luminescent cell viability assay kit was purchased from Promega (Madison, WI, USA). All reagents were used directly as received without any further purification. Human esophagus carcinoma cells (Eca-109) were purchased from the Cell Bank of the Chinese Academy of Science (Shanghai, China).

## 2.2. Synthesis of HMNSs

The HMNSs were synthesized according to Ref. [23] with a slight modification. Briefly, 2 mmol of $FeCl_3 \cdot 6H_2O$ and 20 mmol of $NH_4Ac$ were dissolved in 25 mL of ethylene glycol. As the mixture changed into a clear solution, it was transferred to a Teflon®-lined autoclave and heated to 200°C in a muffle furnace. After reaction at 200°C for 12 h, the product was cooled to room temperature and washed with ethanol and water. The black precipitates were then dried in a vacuum oven at 50°C for 20 h.

## 2.3. Synthesis of GQDs

The GQDs were synthesized according to Ref. [24] with a slight modification, and detailed below. Five grams of L-glutamic acid were placed in a glass beaker and heated to 250 °C in a muffle furnace and then maintained at this temperature for 3.5 h. After the sample was cooled to room temperature, distilled water (30 mL) was added to the sample and sonicated for approximately 10 min. The obtained suspension was centrifuged and the supernatant (GQDs) was collected for freeze drying.

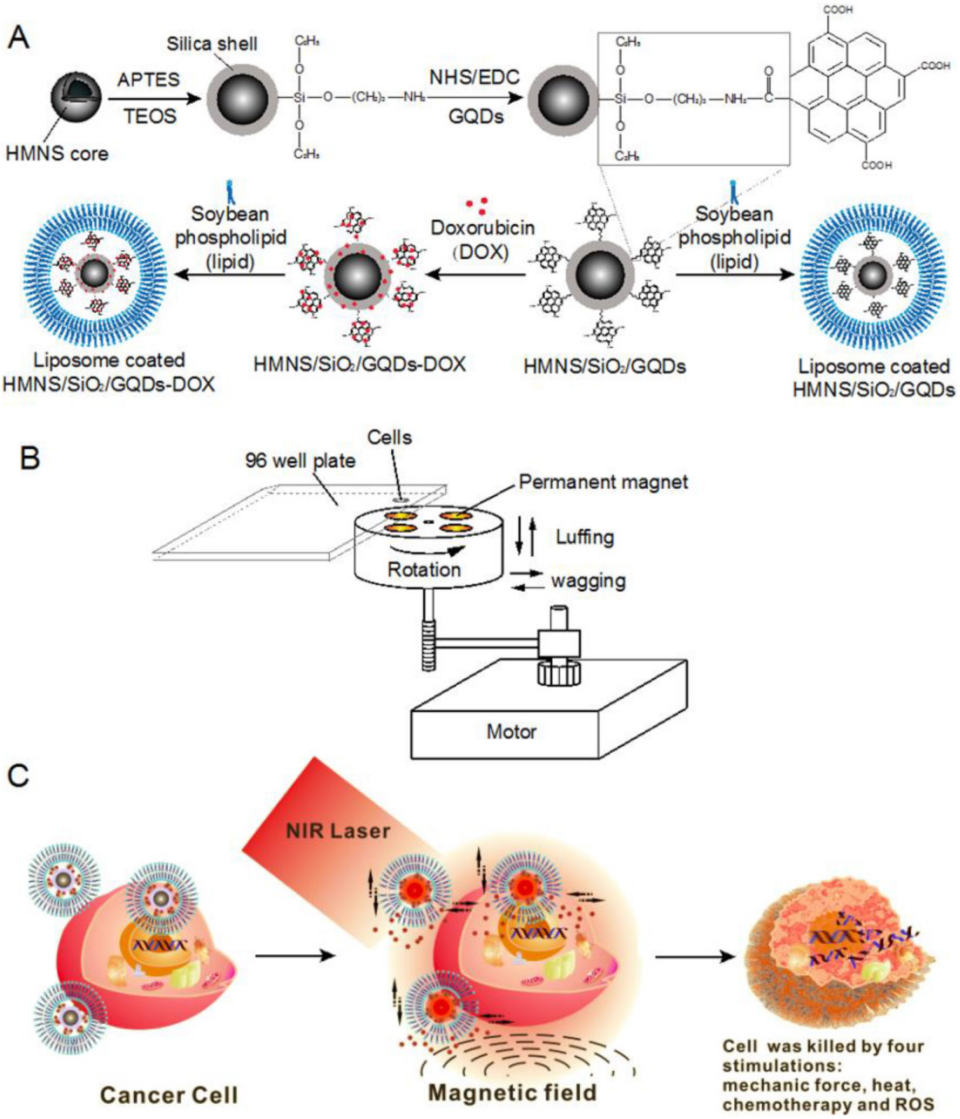


**Figure 1.** Schematic of doxorubicin hydrochloride (DOX)-loaded nanocomposites [hollow magnetic nanosphere (HMNS)/$SiO_2$/graphene quantum dots (GQDs)-DOX] that kill a cancer cell upon exposure to a dynamic magnetic field and near-infrared (NIR) laser irradiation. (A) The formation of liposome-coated HMNS/$SiO_2$/GQDs-DOX nanocomposites. (B) The experimental setup of the dynamic magnetic field. Cells (96-well plate) are placed 1.4 cm above the magnets possessing a magnetic strength of 45.3±0.5 mT and a rotation and swing of 2000 r/min. (C) The nanocomposites obtained exhibit multimodal therapy (mechanical force + heat + chemotherapy + reactive oxygen species) in cancer treatment when treated with an external magnetic field and NIR laser irradiation.

### 2.4. Coating the HMNSs with silica shells, GQDs and lipid layers

The experimental procedures are shown in Figure 1A. In a typical preparation, 1 mg of HMNSs was dispersed in 2 mL of alkaline solution (pH=9–10), and mixed with 100 μL of TEOS (containing 25% ethanol) and 44 μL of APTES. The mixture was vigorously stirred for at least 2 h, and the precipitates were collected by magnetic separation to obtain silica-coated HMNSs (HMNS/$SiO_2$). To further coat these with GQDs, 5 mg of GQDs was dissolved in 2 mL of distilled water in which 4.6 mg of EDC and 2.8 mg of NHS were subsequently added. After stirring for 1 h, the mixture containing GQDs, EDC, and NHS was added into the suspension of HMNS/$SiO_2$ and incubated at room temperature overnight. The HMNS/$SiO_2$/GQDs nanocomposites were collected by magnetic separation and washed three times with water. The amount of GQDs adsorbed by the HMNS/$SiO_2$ was measured based on a standard curve of GQDs (Supplementary Material: Figure S1A).

To improve the dispersion stability of these nanoparticles (except GQDs) in aqueous solution, HMNSs, HMNS/$SiO_2$, and HMNS/$SiO_2$/GQDs were coated with liposomes (Figure 1A) and stabilized with PVP. In a typical experiment, soybean phospholipids (5 mg) were dissolved in chloroform (0.5 mL) in a round-bottomed flask and dried via rotary evaporation to make a thin film. One milliliter of the nanoparticle aqueous suspension containing 1 mg/mL of HMNSs was added into the flask to hydrate the dry lipid film, followed by 30 min of gentle shaking and 3 min of sonication. To further improve the stability of the liposome-coated nanoparticle suspension, PVP was added into the suspension and sonicated for ~3 min. The concentrations of HMNSs, lipids, and PVP in the mixture suspension were 0.5, 2.5, and 20 mg/mL, respectively.

In the following sections, the Liposome-coated HMNSs, HMNS/$SiO_2$, and HMNS/$SiO_2$/GQDs are abbreviated as LP-HMNSs, LP-HMNS/$SiO_2$, and LP-HMNS/$SiO_2$/GQDs, respectively.

### 2.5. Characterization

The morphologies of the HMNSs before and after coating with liposomes, GQDs, HMNS/$SiO_2$, and HMNS/$SiO_2$/GQDs were observed using a high-resolution transmission electron microscope (HRTEM) (JEOL-2010, Japan) equipped with an energy dispersive X-ray spectrometer (EDS) (Oxford) analysis system and operated at 200 kV. Size distributions of the samples were determined by HRTEM analysis over 120 particles for each sample using the software provided with the HRTEM system. X-ray diffraction (XRD) analyses were performed on a Rigaku D/max 2550 VB/PC X-ray diffraction analyzer (Tokyo, Japan) using Cu $K_\alpha$ radiation at an acceleration voltage of 40 kV in the range of Bragg angles ($2\theta$) from 10° to 90°. The room-temperature magnetic properties were characterized using a vibrating sample magnetometer (Physical Property Measurement System from Quantum Design, USA) with a maximum applied field of 1.8 T. The absorption spectra were obtained by using a diode array spectrophotometer (UV-2102PC; Unico, Shanghai, China) with a deuterium lamp source.

### 2.6. Measurement of the nanoparticle photothermal conversion under laser irradiation

The temperatures of the four types of aqueous nanoparticle suspensions (LP-HMNSs, LP-HMNS/$SiO_2$, LP-HMNS/$SiO_2$/GQDs and GQDs,) were measured upon laser irradiation in the same manner as described in our previous work [12]. Two lasers (Shanghai Inter-Diff Optoelectronics Tech. Co., Ltd., Shanghai, China) with wavelengths of 671 nm (power density, 0.2 W/$cm^2$) and 808 nm (power density, 0.25 W/$cm^2$) were used to irradiate the aqueous nanoparticle suspensions. The detailed methods are shown in the Supplementary Material.

### 2.7. Measurement of the intracellular ROS generated by the nanoparticles under laser irradiation

The intracellular ROS levels generated by LP-HMNSs and LP-HMNS/$SiO_2$/GQDs upon laser irradiation were measured in the same manner as described in our previous work [25]. The detailed methods are shown in the Supplementary Material.

### 2.8. Loading of DOX, drug release in aqueous solution as well as intracellular drug release

In a typical experiment, 0.5 mg of HMNSs was incubated with 2 mL of aqueous DOX solution (0.5 mg/mL) at room temperature for at least 12 h, from which the precipitates were collected by magnetic separation. The method of incorporating DOX into HMNS/$SiO_2$ and HMNS/$SiO_2$/GQDs was the same as described previously. The absorption spectra of the original DOX solution and the supernatant solutions of the DOX-nanoparticle mixture after centrifugation were obtained using the diode array spectrophotometer. The DOX content in the nanoparticles was measured based on a standard curve of DOX (Supplementary Material: Figure S1B). For the cell experiments, the DOX-loaded nanoparticles were stabilized with the liposomes and PVP using the preparation method described in the section 2.4.

The release rates of DOX from the DOX-loaded HMNS/$SiO_2$/GQDs in aqueous solution and in cells

(intracellular drug release) were performed, respectively. The experimental details were shown in Supplementary Materials.

### 2.9 The toxicity of the nanocomposoites to cells

LP-HMNSs and LP-HMNS/$SiO_2$/GQDs were major drug carriers studied in this work. The cell uptake and toxicity of these nanocomposites upon incubation were investigated. The experimental details are shown in Supplementary Materials.

### 2.10. Cell destruction by magnetic field-mediated mechanical stimulation

#### 2.10.1. Magnetic field

As shown in Figure 1B, four permanent magnets are evenly positioned and fixed on a wooden disk. The disk on a rotational axis is driven by a motor. During rotation, the disk can also move in axial and radial directions simultaneously. The cells are seeded into a 96-well plate and placed 1.4 cm above the disk, where the magnetic field intensity on the cells is measured to be 45.3±0.5 mT. The rotation and swing of the magnets are 2000 revolutions and 2000 times per minute, respectively.

#### 2.10.2. Magnetic field-mediated mechanical stimulation

Before the cell experiments, we measured the temperature increase of the HMNS aqueous suspensions as a function of magnetic field stimulation. Briefly, 200 μL of LP-HMNS aqueous suspension dispersed by PVP was placed in small glass tubes, where the concentrations of HMNSs, lipids and PVP were 1, 5, and 20 mg/mL, respectively. The initial temperature was maintained at 25.5±0.10°C, and the suspension was exposed to the magnetic field for 20 min. During exposure, a chromel-alumel thermocouple thermometer equipped with a probe as mentioned above was used for the temperature measurements.

For the cell experiments, the Eca-109 cells were cultured at a density of ~$1\times10^4$ cells/well in two wells of a 96-well plate that were located on the diagonal line of the 96-well plate. Twenty-four hours after culture, the medium was removed and 100 μL of serum-free RPMI-1640 medium (with 20 mg/mL of PVP) containing LP-HMNSs was added into one of the two wells, where the concentration of HMNSs in the cells was maintained at 0.5 mg/mL. 100 μL of serum-free RPMI-1640 medium was added into anther well. After 5 min, 30 min and 2 h of incubation times, the well containing HMNSs was exposed to a magnetic field for 20 or 60 min. Another well containing only cells but not exposed to the magnetic field was used as a control. The other controls included the following: an identical 96-well plate containing two wells of cells (in which only one well contained nanoparticles) that was not exposed to the magnetic field, and the cells containing lipids (2.5 mg/mL) and PVP (20 mg/mL) but without HMNSs that were exposed to the magnetic field. After the treatment, the culture medium was removed and replaced with fresh medium. Cells were then continuously cultured at 37°C for 1 h.

The temperature of the cells at the beginning of the magnetic field exposure was maintained at 25°C, and each experiment was repeated six to eight times (one to three times for the qualitative assay, and five times for the quantitative assay). For the cell structure assay [transmission electron microscope (TEM) observation], each experiment was repeated 12–16 times. Cells were then collected from the experiments comprising 12–16 times by trypsin digestion for subsequent histological analysis.

### 2.11. Cell destruction induced by NIR laser irradiation

The experiments were performed in 96-well plates using the same method as described in our previous work [12]. The detailed methods are shown in the Supporting Information.

### 2.12. Cell destruction induced by both magnetic field and NIR laser irradiation

The experimental procedures are illustrated in Figure 1C. The Eca-109 cells were cultured in two wells, each in a 96-well plate at a density of ~$1\times10^4$ cells/well. Magnetic nanoparticles (e.g., LP-HMNSs) were added to one well in the same manner as described in the previous sections. In one group, the wells containing nanoparticles were first irradiated with a 671- or 808-nm laser for 20 min, and then exposed to the magnetic field for 20 min. In the other group, the wells containing nanoparticles were first exposed to the magnetic field for 20 min and then irradiated with the laser for 20 min. After the treatment, the culture medium was removed and replaced with fresh medium. Cells were then continuously cultured at 37°C for 1 h. Each experiment was repeated six to eight times.

### 2.13. Cell viability measurements

The cell viabilities in the experiments presented in the three previous sections were assessed as follows: after exposure to the magnetic field or/and laser irradiation, cells were cultured for 1 h, as described above. The culture medium was replaced with 200 μL of dye solution (containing 196 μL staining buffer, 1 μL Hoechst 3334, and 3 μL PI) and incubated at 4°C for 30 min. The cell viability was then qualitatively assayed based on the cell fluorescence (excitation

wavelength, 365 nm), which was observed using an upright fluorescent microscope (Nikon Eclipse TE2000, Japan).

The quantitative assay of cell viability was as follows. After the cells were treated with the magnetic field and/or laser irradiation, and then further cultured for 1 h as mentioned above, the culture medium was removed and the cells were gently washed with phosphate- buffered saline. The CellTitre-Glo® reagent (100 μL) was added to each well and agitated for 5 min at room temperature. The cell viability was assayed based on the cell luminescent intensity (emission wavelength: 500 nm), which was recorded using SpectraMax M5 Multi-Mode Microplate Readers.

### 2.14. Histological analysis

The cell structures were analyzed using TEM as described in a previous work [12]. Briefly, after cells were collected by trypsin digestion, they were fixed with 2.5% glutaraldehyde and then treated with 1% $OSO_4$ solution, ethanol solution, ethanol:acetone solution, acetone solution, and the mixture solution of acetone:epoxide resin. The cells were then embedded in pure epoxide resin and the ultrathin (70-nm) sections of the embedded specimens were cut with an ultramicrotome (Lecia EM uc6) using a diamond knife. The thin sections were observed with a TEM (JEOL, JEM-1230) at an accelerating voltage of 80 kV.

### 2.15. Statistical analysis

Statistical significance was determined by one-way analysis of variance (ANOVA) followed by Tukey's post-hoc test. The P-value <0.05 was considered statistically significant. P<0.01 and P<0.001 were considered as highly and extremely highly significant statistical differences, respectively.

## 3. Results and Discussion

### 3.1. Characterization of the HMNSs

HMNSs are spherical in shape with a narrow size distribution (250–550 nm) as shown in Figures 2A (a, b) and Figure 2B. Thery are also found hollow and porous (Figure 2A (b)).These features are ideally suitable for drug loading. The shells of these HMNSs are formed by the aggregation of small nanoparticles with only several nanometers in diameter. The average size of HMNSs is 391.30±66.62 nm with a shell thickness that ranges from 50 to 150 nm and a pore size of 10 nm, determined by using the analysis software available in the HRTEM system. After coating with lipid shells, the surfaces of the LP-HMNSs appear quite rough, a morphology that is different from those of the bare HMNSs (Figure 2A (c)). EDS results show only Fe and O in these nanospheres (Figure 2C), while the XRD pattern confirms their $Fe_3O_4$ cubic structure (JCPDS 79-0419) (Figure 2D). The saturation magnetization data of these hollow nanospheres shows a strong moment of 80 emu/g. The remanence and coercivity of HMNSs are close to zero, showing the characteristic of superparamagnetism (Figure 2E).

### 3.2. Efficacy of cancer cell killing by LP-HMNSs through magnetic field-mediated mechanical stimuli

#### 3.2.1. Qualitative analysis of cell viabilities

As has been shown previously, PI dye can only penetrate into damaged or dead cells, where it binds to DNA and emits red fluorescence (~617 nm wavelength), whereas Hoechst 33342 (a blue fluorescent dye) can penetrate both living and dead cells. The double-stain technique using Hoechst 33342/PI apoptosis detection reagents can therefore be used as a quick visual evaluation of cancer cell destruction by the magnetic field-mediated mechanical stimuli. To improve HMNSs dispersion in aqueous solution and their binding to the cells, they were coated with liposomes composed of soya lecithin and dispersed in fresh 1640 medium containing 20 mg/mL of PVP, where the mass ratio of HMNSs to lipids was 1:5. As shown in Figure 3A, when incubating Eca-109 cells with LP-HMNSs (HMNSs: 0.5 mg/mL) at 37°C for 5 min and subsequently washed with culture medium, nearly all cells are decorated with a large amount of nanoparticles. It can also be seen that the size and morphology of the cells incubated with LP-HMNSs are similar to those not incubated with the magnetic nanoparticles. Importantly, most cells were dyed with blue fluorescence after adding the Hoechst 33342/PI reagents. Furthermore, the results from the cells incubated with the LP-HMNSs for 20 min and 2.5 h are similar to those incubated with the magnetic nanoparticles for 5 min. These results indicate that the LP-HMNSs can be well adsorbed by the cancer cells in a short time without obvious damage.

As shown in Figure 3B, when incubating the Eca-109 cells with LP-HMNSs (HMNSs: 0.5 mg/mL) for 5 min, and exposing them to the rotational and swing of the magnets for 20 min (and then continually cultured at 37°C for 1 h), approximately one fifth of the total amount of the cells have been killed, as evidenced by their emission of red fluorescence (dyed with the Hoechst 33342/PI). As can be seen in this figure, more than two-fifths of the cells containing the LP-HMNSs appears dead when exposed to the same magnetic field for 60 min (and then continually cultured for 1 h). When the cells were incubated with LP-HMNSs for 30 min and 2 h and then exposed to the magnetic field for 20 min (and continually cultured for 1 h), about one fifth and one fourth of the total amount of the cells have died, respectively.

These results suggest prolonged incubation results in higher uptake of the nanocomposites by the cells leading to more cells destruction by the magnetic field-mediated mechanical stimuli. The bright-field images also show considerable shrinkage of some cells by red fluoresce.

In the control experiment, nearly all cells were seen to survive upon incubation with the stabilizers (lipid and PVP) when exposed to a magnetic field for 20 min. These results are consistent that only the cells containing HMNSs can be effectively damaged by magnetic field-mediated mechanical stimuli.

### 3.2.2. Quantitative analysis of cell viabilities

The concentration of adenosine trisphosphate (ATP) is directly proportional to the number of living cells. The cell viability was investigated by ATP measurement using a CellTiter-Glo® reagent. The concentration of LP-HMNSs and cell culture protocols were the same as described previously. As shown in Figure 3C, when incubating cells with LP-HMNSs (HMNSs: 0.5 mg/mL) for 5 min and subsequently exposed to a magnetic field for 20 and 60 min, the average cell viabilities are 73.99±5.36 and 57.84±6.94%, respectively ($P<0.01$ between these two groups). This indicates increased cell-killing efficiency of the LP-HMNSs with prolonged exposure to magnetic field-mediated mechanical stimuli. Upon incubating the cells with LP-HMNSs (HMNSs: 0.5 mg/mL) for 30 min or 2 h and subsequently exposed to a magnetic field for 20 min, the cell viability was found to be 76.80±4.53 or 70.39±7.92%, respectively. There are no significant differences in the cell viability between these two groups.

The cell viabilities of the control groups were found to range from 99.50 to 105.35% for cells incubated with LP-HMNSs but not exposed to the magnetic field, and for those incubated with the stabilizers (lipid and PVP) only, with and without a magnetic field. These results are in agreement with those using the double fluorescence staining method described in the previous section, and further demonstrating the efficacy of HMNSs cell killing by applying a magnetic field. The temperature of 200 μL LP-HMNS aqueous suspension (HMNSs: 0.5 mg/mL) was remained at 25°C when exposed to the magnetic field for 20 min. This implies that the cells were killed only by the mechanical force of the magnetic particles under the magnetic field.

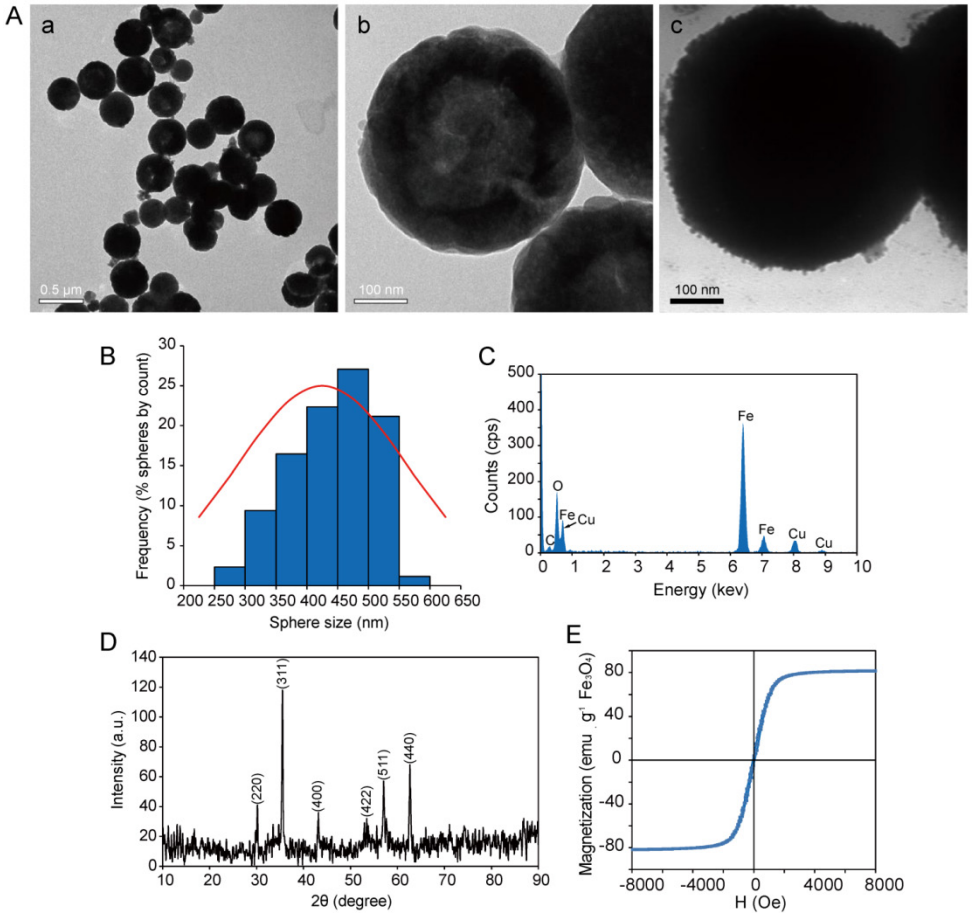


**Figure 2.** Characterization of HMNSs. (A) HRTEM images of HMNSs (a: low magnification, b: high magnification) and (c) LP-HMNSs. (B) Size distribution of HMNSs. (C) Energy dispersive X-ray spectra, (D) X-ray diffraction pattern, and (E) magnetization of HMNSs.

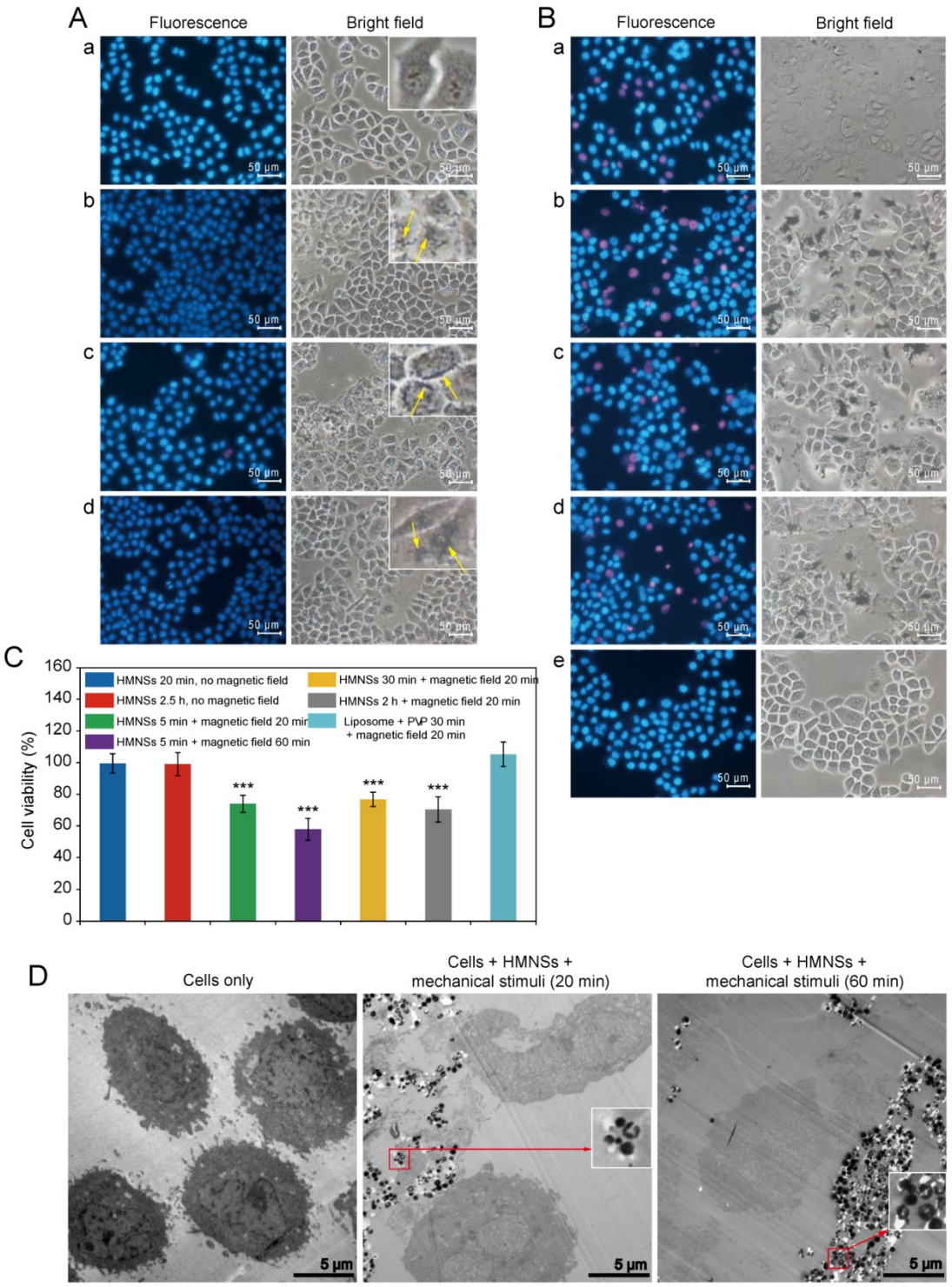


**Figure 3.** LP-HMNSs triggering Eca-109 cell death induced by magnetic field-mediated mechanical stimuli and controls. (A) The viability of the Eca-019 cells after being incubated with the LP-HMNSs without the magnetic field: (a) cells alone; cells incubated with the LP-HMNSs for (b) 5, (c) 20, and (d) 150 min. The arrows point to the HMNSs. (B) Qualitative detection of the magnetic field-mediated mechanical stimuli, triggering cancer cell death: cells incubated with the LP-HMNSs for 5 min and subsequently exposed to the magnetic field for (a) 20 and (b) 60 min. Cells incubated with the LP-HMNSs for (c) 30 min and (d) 2 h and subsequently exposed to the magnetic field for 20 min. (e) Cells incubated with the liposomes and PVP for 30 min and subsequently stimulated by the magnetic field for 20 min. (C) Quantitative analysis of the viability of cells incubated with LP-HMNSs upon magnetic field-mediated mechanical stimuli for different time periods and controls. The times that the cells were incubated with the materials and subsequently exposed to the magnetic field are listed to the right of the color symbols, respectively. (D) TEM images of cells destroyed by magnetic field-mediated mechanical stimulation: (left) cells alone; (middle) cells incubated with LP-HMNSs for 5 min and then stimulated by the magnetic field for 20 min; (right) cells incubated with HMNS for 5 min and then stimulated by the magnetic field for 60 min. For the cell experiments, the LP-HMNSs were dispersed in culture medium containing PVP. The concentrations of HMNSs, lipids, and PVP in the culture medium were 0.5, 2.5, and 20 mg/mL, respectively. The significance level observed is *** $P<0.001$, compared with the group values of cells incubated with LP-HMNSs for 20 min without a magnetic field. Data are expressed as the mean ± the standard deviation. The error bars are based on the results of five experiments per group.

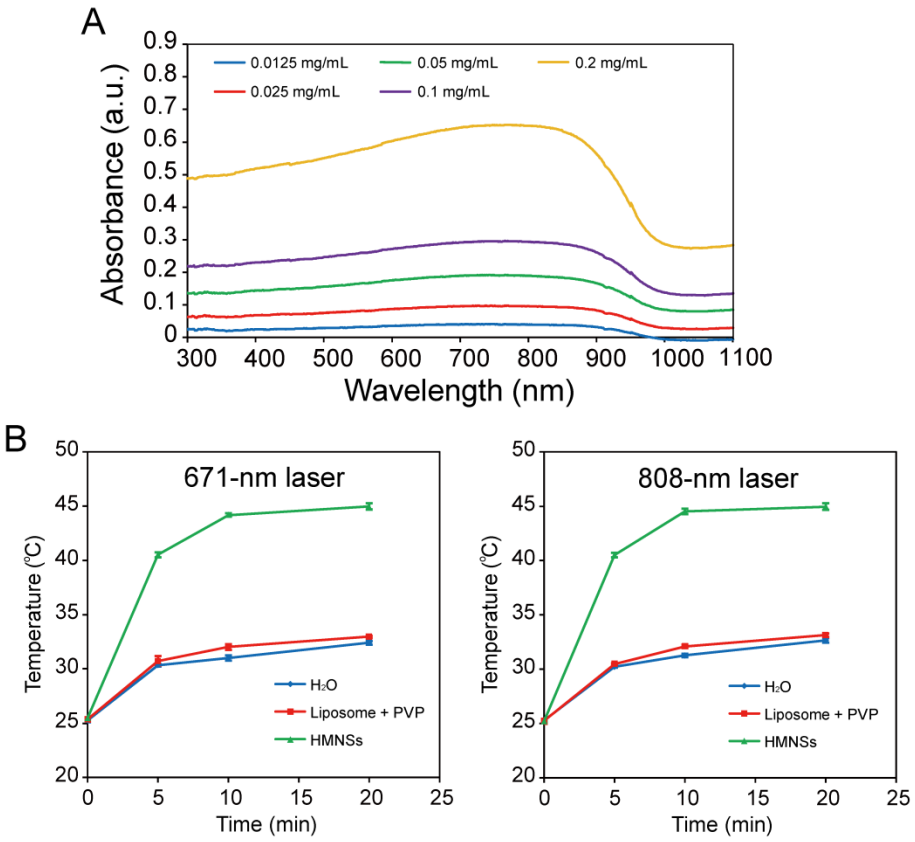


**Figure 4.** Absorption spectra and photothermal conversion of LP-HMNSs. (A) Absorption spectra of the LP-HMNSs in water with different concentrations of HMNSs. (B) Temperature increase of the LP-HMNSs in water upon exposure to a 671- and 808-nm laser. The LP-HMNSs were dispersed in distilled water containing PVP. For absorption spectrum detections, the mass ratio of HMNSs to lipids to PVP was 1:5:40 (the concentrations of HMNPs are indicated in this figure). The aqueous solutions containing liposomes and PVP were used for setting up the base line. For photothermal conversion detections, the concentrations of HMNSs, lipids, and PVP in water were 0.5, 2.5, and 20 mg/mL, respectively.

### 3.2.3. Histology analysis after the mechanical stimuli

To further investigate the effect of magnetic-mediated mechanical stimulation on cell structures, cells were embedded in an epoxide resin and cut into ultrathin sections for TEM analysis. As shown in Figure 3D, the Eca-109 cells without treatment exhibit intact intracellular structures (e.g., the nucleus can be observed clearly) with uniform size. However, for LP-HMNSs containing cells (HMNSs: 0.5 mg/mL) exposed to the magnetic field for 20 min, the frameworks exhibit obvious damage with discontinuous cell membrane. As can also be see in this figure, the intracellular structure is incompact, and the integrity of the nuclear membrane is no longer well defined. For 60 min exposure time, some cells were seen to be seriously damaged with severely altered cellular morphologies. Nonetheless, HMNSs in cells remain well defined with the hollow structures (Figure 3D inserts).

A living cell is a high-precision but fragile system that is unable to bear strong external stimulation (e.g., acid, alkali). The cell membrane or/and other sub-cellular structures are easily broken by external mechanical stimulation, resulting in programmed or direct cell death.

## 3.3. Effect of NIR laser irradiation on cancer cells containing LP-HMNSs

HMNSs was found to efficiently convert NIR laser light energy into heat, suggesting a highly effective means for cancer cell killing via the photothermal effect. This effect can also be combined with the magnetic-mediated mechanical stimulation for further improved efficiency.

### 3.3.1. Photothermal conversion of LP-HMNSs upon laser irradiation

LP-HMNSs in aqueous solution have a strong optical absorption between ~ 600 nm and 1000 nm (Figure 4A). Their absorption coefficients at 671 and 808 nm were found to be 3.35±0.39 and 3.37±0.40 $L \cdot g^{-1} \cdot cm^{-1}$, respectively. When the LP-HMNSs were dispersed in 200 μL of distilled water and irradiated with a 671- or 808-nm laser for 20 min, the aqueous temperature increased rapidly in the first 5–10 min and then gradually leveled off during the subsequent irradiation (Figure 4B). For example, the temperature of the solution (initial temperature: 25.3±0.10°C) con-

taining 0.5 mg/mL of HMNSs increased by 15°C after 5 min of 671-nm irradiation; and by 18°C and 19°C after 10 min and 20 min of 671-nm irradiation, respectively. The temperature increase of the LP-HMNS suspension upon 671-nm laser irradiation was not significantly different when exposed to 808-nm laser irradiation owing to their similar absorption coefficients at these wave lengths. Cancer cells can be killed at temperatures higher than 42.5°C [26]. Therefore, cancer cell growth may be effectively inhibited by the photothermal effect of HMNSs. The photothermal conversion efficiency of HMNSs upon 671-nm laser irradiation was 21.9%. The temperatures of the controls, i.e., 200 μL of distilled water and stabilizers (2.5 mg/mL liposomes + 20 mg/mL PVP), increased by no more than 7.0 and 8.0°C after 20 min of 671- and 808-nm laser irradiation, respectively.

The Eca-109 cells containing the LP-HMNSs (HMNSs: 0.5 mg/mL) were irradiated with the 671-nm laser for 20 min. Subsequently, the cell structures were found to be distinctly changed compared with the untreated cells. A typical image is shown in Figure 5A. As can be seen in this figure, the nuclei are severely damaged and membrane roughened, although the cell frames can be observed after irradiation. Some cells are also seen to be reduced in size compared to the untreated cells.

### 3.3.2. Qualitative analysis of cell viabilities after photothermal stimulation using LP-HMNSs

Hoechst 33342/PI double stain apoptosis detection reagents were used to visually analyze cell viability (Figure 3C). The Eca-109 cells were incubated with LP-HMNSs (HMNSs: 0.5 mg/mL) and irradiated using the 671-nm laser for 20 min. Upon one hour post-irradiation, many cells (~30%) emitted red fluorescence, indicating cell death. As shown in Figure 5B (a), the PI reagent has penetrated the damaged membrane of the cells. Similar results were observed when cells were irradiated at 808 nm (Figure 5B(b)). Nearly all the cancer cells containing 2.5 mg/mL of liposomes and 20 mg/mL of PVP emitted blue fluorescence with (both wavelengths) or without laser irradiation (Figure 5B(c) and Figure 5B(d)). These results indicate effective cancer cell killing by HMNSs upon NIR laser irradiation, whereas the liposomes and PVP, with or without laser irradiation, show insignificant effects.

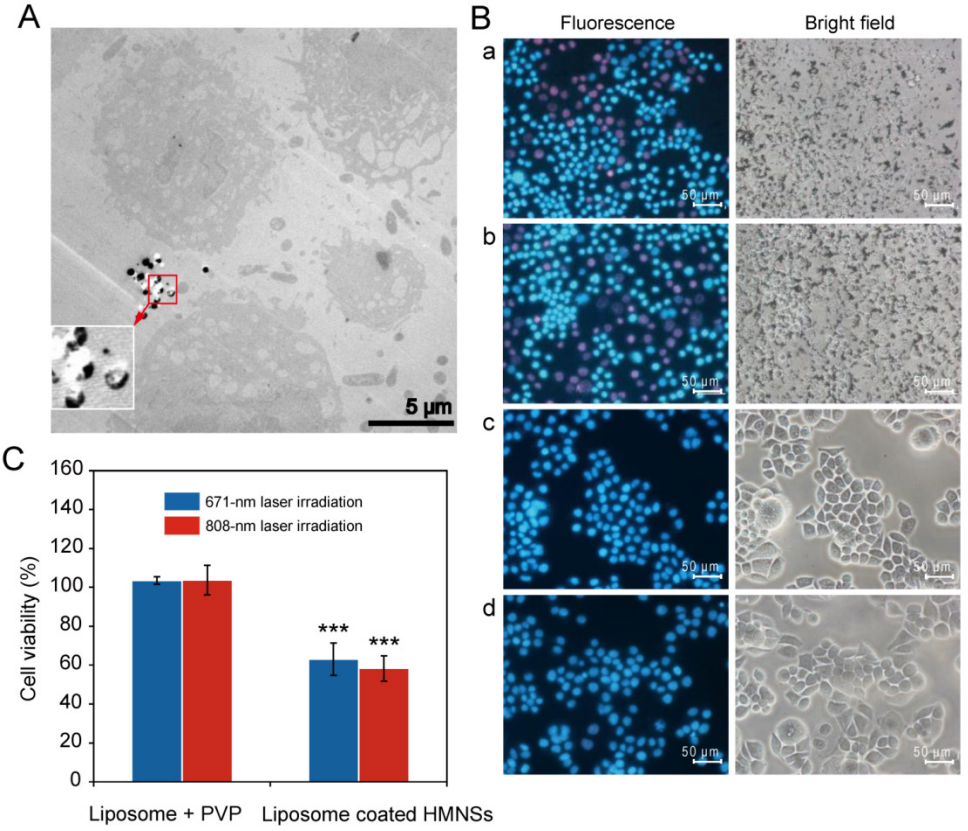


**Figure 5.** The thermal stimuli of LP-HMNSs upon laser irradiation triggering Eca-109 cell death and the results of the controls. (A) TEM images of cells destroyed by 671-nm laser irradiation. Cells were incubated with the LP-HMNSs for 5 min and then irradiated by the laser for 20 min. (B) Qualitative detection of the LP-HMNSs photothermal stimuli upon laser irradiation triggering cancer cell death, wherein cells containing LP-HMNSs were irradiated by a (a) 671- and (b) 808-nm laser for 20 min, and the cells containing blank liposomes (liposomes: 2.5 mg/mL) and PVP (20 mg/mL) were irradiated by a (c) 671- and (d) 808-nm laser for 20 min. (C) Quantitative analysis of the viability of cells incubated with LP-HMNSs and irradiated with 671- and 808-nm laser irradiation for 20 min. The LP-HMNSs were dispersed in water (for temperature detection) and a culture medium (for cell experiments) containing PVP. The concentrations of HMNSs, lipids, and PVP in water or the culture medium were 0.5, 2.5, and 20 mg/mL, respectively. The significance level observed was *** $P<0.001$, in comparison with the group values of cells incubated with liposomes and PVP with 671-nm laser irradiation. Error bars indicate the standard error of the mean based on three (for temperature detection) and five (for cell experiments) experiments per group.

### 3.3.3. Quantitative analysis of cell viability upon photothermal stimulation by LP-HMNSs

Cell viability quantification through ATP content in the cells was used to evaluate the efficiency of laser-induced cell killing by HMNSs. As shown in Figure 5C, the averages of cell viabilities for the Eca-109 cells are 63.12±8.29 and 58.38±6.54%, respectively, when incubated with the LP-HMNSs (HMNSs: 0.5 mg/mL) and irradiated by the 671 nm or 808 nm laser for 20 min. Conversely, about 100% average viabilities of the cells were observed after incubation with liposomes (2.5 mg/mL) and PVP (20 mg/mL), with or without laser irradiation. The same was also found for the blank cells with laser irradiation (data not shown).

## 3.4. Effect of magnetic field-mediated mechanical stimulation (MFMS) and NIR laser irradiation on cells containing LP-HMNSs

Two methods were applied to destroy the cancer cells. The cells were irradiated with the NIR laser first, followed by magnetic field-mediated mechanical stimulation (MFMS), or vice versa.

### 3.4.1. Qualitative analysis of cell viabilities

The Eca-109 cells were incubated with LP-HMNSs (HMNSs: 0.5 mg/mL). They were then irradiated with the 671 nm laser for 20 min. Subsequently, these cells were exposed to the magnetic field for 20 min. With the addition of Hoechst 33342/PI double stain reagents, most of the cells emitted red fluorescence (Figure 6A(a)). The number of red-fluorescing cells was found to be significantly higher than those either treated with the magnetic field (Figure 3B(a)) or laser irradiated alone (Figure 5B(a)). Similar results were found for the cells irradiated with the 808-nm laser and then exposed to the magnetic field (Figure 6A(b)).

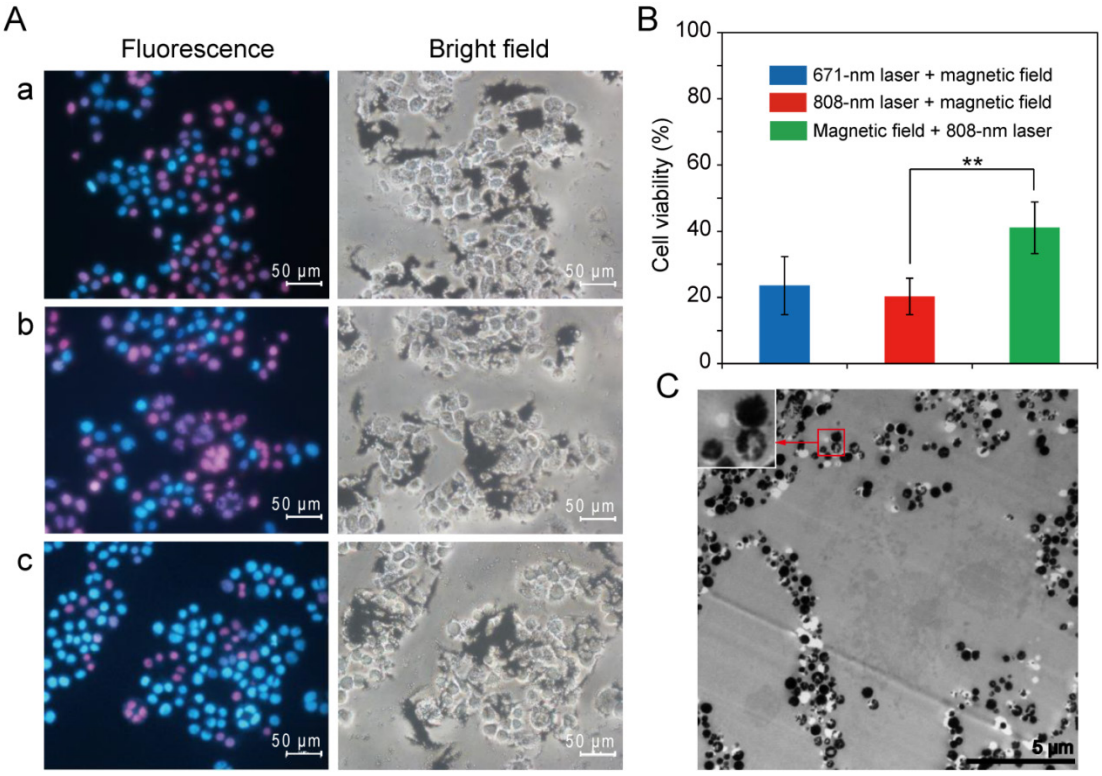


**Figure 6.** LP-HMNSs triggering Eca-109 cell death induced by both NIR laser irradiation and magnetic field-mediated mechanical stimuli. (A) Qualitative detection. The cells were incubated with the LP-HMNSs and then irradiated by (a) 671- or (b) 808-nm laser for 20 min and subsequently exposed to the magnetic field for 20 min. (c) The cells containing the LP-HMNSs were exposed to the magnetic field for 20 min and then irradiated by the 808-nm laser for 20 min. (B) Quantitative analysis. (C) TEM images of cells destroyed by 671-nm laser irradiation (20 min) and subsequent magnetic field-mediated mechanical stimuli (20 min). The LP-HMNSs were dispersed in a culture medium containing PVP. The concentrations of HMNSs, lipids, and PVP in the culture medium were 0.5, 2.5, and 20 mg/mL, respectively. The significance level observed was ** $P<0.01$, in comparison with the group values of cells incubated with LP-HMNSs and subsequently treated with the reversed order of laser irradiation and magnetic field stimulation. Data are expressed as the mean ± the standard deviation. The error bars are based on five experiments per group.

### 3.4.2. Quantitative analysis of cell viabilities

The CellTiter-Glo® reagent was used to measure the ATP content of cells after the treatments with the two stimuli. As shown in Figure 6B, upon irradiation with the 671 nm laser, then exposed to the magnetic field (20 min for each stimulation), the Eca-109 cells containing LP-HMNSs (0.5 mg/mL) show cell viability of only 23.60±8.77%. When the cells were treated with the 808-nm laser and then exposed to the magnetic field or, conversely, treated with the magnetic field and then exposed to the 808-nm laser, the cell viabilities were 20.35±5.45 and 41.06±7.74%, respectively, indicating a significant difference in cell viability when switching the order of the treatment. As shown in Figure 6A(c), most of the cells that are dyed with red color appear to have died. This is the result of NIR irradiation being more lethal in cell killing than the magneto-mechanical force (see Figures 3 and 5). When the cells are exposed to a weaker stimulus (MFMS) first followed by a stronger one (PTT) the cells are more seriously damaged compared to the treatments with the reversed order. These quantitative assessments of call viability demonstrate the improved effectiveness in cancer therapy by the synergistic effects of PTT and MFMS.

The damage imposed on the cell structure by the two stimuli was observed by TEM. As shown in Figure 6C, upon irradiation by the 671-nm laser for 20 min followed by exposure to a magnetic field for 20 min, the cell structures are severely damaged and physically broken into pieces.

## 3.5. Characterization of HMNS/$SiO_2$, HMNS/$SiO_2$/GQDs, and DOX-loaded HMNS/$SiO_2$/GQDs

### 3.5.1 Morphology, EDS analysis, and magnetic properties of HMNS/$SiO_2$ and HMNS/$SiO_2$/GQD

We selected the commonly used chemotherapy drug DOX as a model anticancer therapeutic for preparation of drug-loaded magnetic nanospheres. We found, however, the DOX-loading efficiency of HMNSs was no more than 2% wt/wt.

To improve the drug-loading efficiency, we coated HMNSs with a silica shell and conjugated them with GQDs. The HRTEM (Figure 7A) and EDS (Figure 7B) studies show well modified HMNSs with the silica shell with a shell thickness about 50 nm. The as-synthesized GQDs were only ~5–10 nm in diameter (Figure 7A). After conjugating HMNSs with GQDs, the surfaces of HMNS/$SiO_2$/GQDs appear to be morphologically roughened compared to the HMNS/$SiO_2$ particles (Figure 7A).

Based on the fluorescence spectra of the GQD solution before and after mixing with the nanoparticles, we calculated that there is 0.42 g of GQDs per 1 g of HMNSs. The saturation magnetizations of HMNS/$SiO_2$ and HMNS/$SiO_2$/GQDs are 17 and 14 emu/g (Figure 7C), respectively, which indicate strong magnetic moments of these nanospheres.

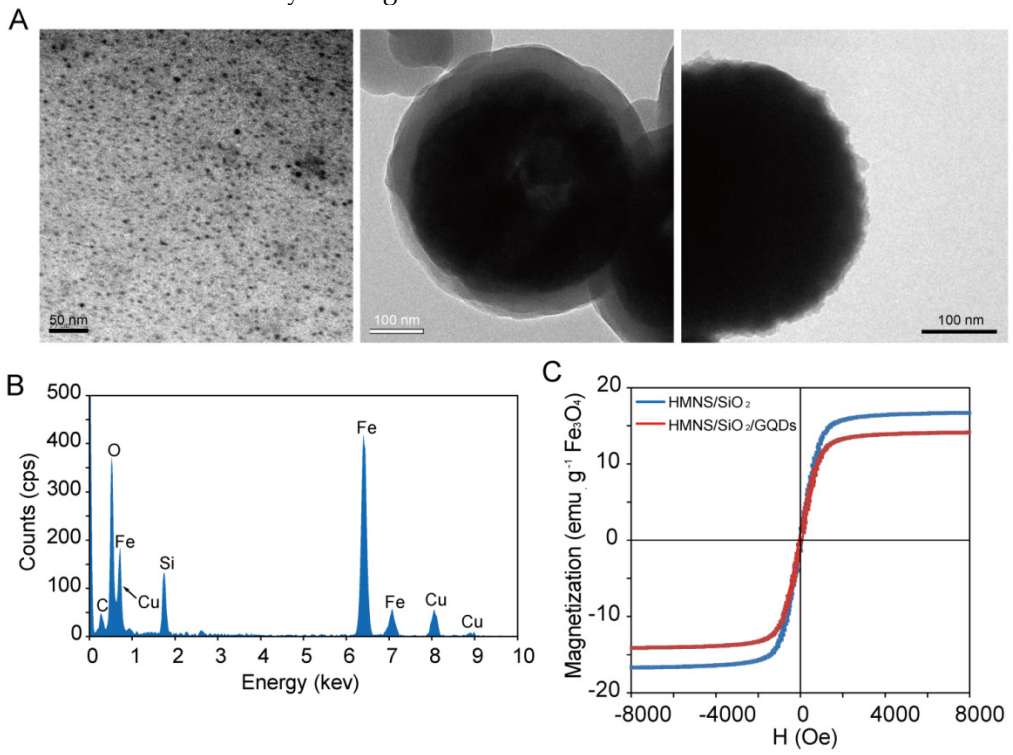


**Figure 7.** Characterization of HMNS/$SiO_2$ and HMNS/$SiO_2$/GQDs. (A) HRTEM images of GQDs (left), HMNS/$SiO_2$ (middle), and HMNS/$SiO_2$/GQDs (right). (B) Energy dispersive X-ray spectrum of the HMNS/$SiO_2$ nanocomposite. (C) Magnetization of HMNS/$SiO_2$ and HMNS/$SiO_2$/GQDs.

GQDs are single- or few-layer carbon nanosheets with only several nanometers in size. These small nanosheets have huge specific surface areas. Therefore, the specific surface area of HMNS/$SiO_2$ will increase upon conjugating with GQD, which will benefit drug loading efficiency.

### 3.5.2. Photothermal conversion of GQDs, LP-HMNS/$SiO_2$, and LP-HMNS/$SiO_2$/GQDs in aqueous solutions upon laser irradiation

We found GQDs efficiently convert NIR laser light energy into heat. As shown in Figure S2, the temperature of 200 μL of GQD aqueous solution, after exposure to 20 min of 671-nm laser irradiation, increases from an initial temperature of 25.1±0.1°C to 33.9±0.5 (GQDs: 0.2 mg/mL) and 42.6±0.2°C (GQDs: 2.5 mg/mL), respectively. The temperature increased more rapidly for the solution of higher GODs concentration. The photothermal conversion efficiency of GQDs upon 671-nm laser irradiation is 23.3%, a sufficiently high heat generation for effective cancer cell killing since cancer cells cannot survive at only higher than 42.5°C [26].

To improve dispersion of HMNS/$SiO_2$ and HMNS/$SiO_2$/GQDs in aqueous solution, they were also coated with liposomes and further stabilized by PVP (see Method). As also shown in Figure 4B and (Supplementary Material: Figure S2), the temperature increase rate of the LP-HMNS/$SiO_2$ is 1–2°C lower than that of the LP-HMNSs. This difference in heating rate is due to the silica shell being unable to convert laser light into heat, limiting the irradiation of the HMNS core. It should be noted that the temperature increase of LP-HMNS/$SiO_2$/GQDs upon 671-nm laser irradiation was more rapid than that of the LP-HMNSs (Figure 4B and Supplementary Material: Figure S2), as a result of heat generation by GQDs on the HMNS/$SiO_2$ surface.

### 3.5.3. Intracellular ROS generated by LP-HMNS/$SiO_2$/GQDs upon laser irradiation

As shown in Figure S3, the average ROS level is 17.92±8.22 times greater than the control (the cells without nanoparticles and irradiation), when the Eca-109 cells are incubated with LP-HMNS/$SiO_2$/GQDs (HMNSs: 0.5 mg/mL, GQDs: 0.2 mg/mL) and irradiated with the 671-nm laser for 20 min. For the un-irradiation group, however, the average ROS level was only 2.36±1.88 times greater than the control. Both $SiO_2$ [27] shell and GQDs [18] after irradiation can generate ROS attributing to this difference. As also shown in Figure S3, the average ROS levels generated by the LP-HMNS/$SiO_2$ with and without 671-nm laser irradiation are 4.39±1.53 and 1.18±0.64 times greater than the control, respectivel, as a reuslt of much higher ROS generated by GQDs than the $SiO_2$ shell. No ROS was found to be generated by HMNSs (data not shown).

### 3.5.4. Drug (DOX) loading of HMNS/$SiO_2$/GQDs and drug release

Both silica shell and GQDs (especially the GQDs) were found to adsorb large amounts of DOX. Figure S4 shows the absorptions of DOX by the HMNS, HMNS/$SiO_2$, and HMNS/$SiO_2$/GQDs nanoparticles. Based on the absorption spectra of the DOX solution before and after mixing with the nanoparticles, we calculated the drug-loadings of the HMNS, HMNS/$SiO_2$, and HMNS/$SiO_2$/GQDs nanoparticles to be 0.02 g, 0.21 g, and 0.66 g of DOX/g HMNSs, respectively. A large amount of DOX was incorporated into the HMNS/$SiO_2$/GQDs nanocomposites, which can be explained by the interactions between the GQDs and DOX, including $\pi$–$\pi$ stacking, hydrogen bonding, and electrostatic interaction.

The release rate of DOX from the DOX-HMNS/$SiO_2$/GQDs system was accelerated by NIR laser irradiation and magnetic field-mediated mechanical stimulation. When the DOX-HMNS/$SiO_2$/GQDs in aqueous solution was irradiated with the 671-nm laser for 20 min, the amount of DOX released from the nanocomposites was 1.3 times higher than that without irradiation (Supplementary Material: Figure S5). Similar behavior was observed in the DOX-HMNS/$SiO_2$/GQDs solutions treated with the magnetic field (data not shown). The intracellular DOX release was significantly affected by the external stimulations. For example, when Eca-109 cells were incubated with the DOX-loaded HMNS/$SiO_2$/GQDs (HMNSs: 0.5 mg/mL, GQDs: 0.2 mg/mL, DOX: 0.3 mg/mL) and irradiated with the 671-nm laser, red fluorescence in cells became increasingly bright with irradiation time (Supplementary Material: Figure S6). For the cells containing the drug-loading system without irradiation, however, only week red fluorescence was observed in cells (Supplementary Material: Figure S6). This is the evidence that the DOX release rate from the nanocomposites in cells can be improved by the NIR laser irradiation.

## 3.6. Effect of DOX-loaded HMNS/$SiO_2$/GQDs on cancer cell viability with magnetic field-mediated mechanical stimulation and NIR laser irradiation

The DOX-loaded HMNS/$SiO_2$/GQDs is a much more lethal cell killing system due to its combined chemotherapeutic, photodynamic, mechanical stress, and photothermal effects.

### 3.6.1 The toxicity of the HMNSs and HMNS/$SiO_2$/GQDs to cells

The toxicities of HMNS/$SiO_2$/GQDs and HMNSs to cells were investigated without any applied external fields. We incubated the Eca-109 cells with LP-HMNS/$SiO_2$/GQDs and LP-HMNSs for different times. The culture medium contained PVP. As a control, the cells were incubated with the mixture solution of liposome and PVP. The concentration of HMNSs, GQDs, lipid and PVP were 0.5, 0.2, 2.5 and 20 mg/mL, respectively. As shown in Figure S7, there is no statistical difference in the cell viability among the LP-HMNS, LP-HMNS/$SiO_2$/GQDs nanocomposite, and the control groups. For example, when the cells were incubated with the samples for 36 h, the cell viabilities in the LP-HMNS and LP-HMNS/$SiO_2$/GQDs nanocomposite groups were 127.62±16.27% and 126.17±13.01%, respectively, quite similar to the control group (121.84±21.03%), indicating good biocompatibility of the drug carriers, which is an important prerequisite for multimodality therapy.

### 3.6.2. Laser irradiation

To investigate the role of GQDs in the HMNS/$SiO_2$/GQDs-DOX nanocomposites for inhibiting cancer cell growth, we incubated the Eca-109 cells with GQDs (0.2 mg/mL), and irradiated the cells with the 671-nm laser. Qualitative analysis using Hoechst 33342/PI double-stain reagents showed clearly that GQDs without irradiation exhibited no phototoxicity to the cells (Supplementary Material: Figure S8A), but sufficient cancer cell killing with laser irradiation (Supplementary Material: Figure S8B). Quantitative analysis showed 8% of the cells was killed after 20 min of 671-nm laser irradiation (Supplementary Material: Figure S8D) for only 0.2 mg/mL of GQDs due to synchronous generation of heat and ROS.

As shown in Figure S8C and S8D in the Supplementary Material, the cell viabilities are 89.46±3.45 and 89.60±2.45%, respectively, with and without 671-nm laser irradiation, when the Eca-109 cells were incubated with DOX (0.3 mg/mL). These results indicate cell killing efficiency by DOX is not enhanced by NIR laser irradiation, but mainly depending on cytotoxicity of the drug.

The phototoxicities of LP-HMNS/$SiO_2$/GQDs to cancer cells are shown in Figure 8A(a) and Figure 8B. As can be seen in these figures, nearly all the cells have survived (viability: 98.87±9.57%) when incubated with the LP-HMNS/$SiO_2$/GQDs (HMNSs: 0.5 mg/mL, GQDs: 0.2 mg/mL) without exposure to laser irradiation. It should be noted that when these cells were irradiated with the 671-nm laser for 20 min, both qualitative (Figure 8A (b)) and quantitative (Figure 8B) analyses show significantly lower cell viability (37.75±12.76%) ($P<0.01$) than that treated with LP-HMNSs (Figure 5B (a) and Figure 5C). It is also lower than those treated with GQDs and laser irradiation (Supplementary Material: Figure S8D). These differences are directly resulted from the simultaneous photothermal and photodynamic effects exerted by HMNS/$SiO_2$/GQDs. In addition, we found fast uptake of LP-HMNS/$SiO_2$/GQDs by the cells. For example, when the cancer cells were incubated with the LP-HMNS/$SiO_2$/GQDs (HMNSs: 0.5 mg/mL, GQDs: 0.2 mg/mL) for 30 min, a large amount of nanocomposites in cells was observed clearly by the confocal fluorescent images (Supplementary Material: Figure S9). This indicates that the nanocomposites can directly release heat and ROS into the cell interior space, respobsible for high phototoxicity to cells. 1.9%21 mor-bearing mice werehrella d with intact chlorella and irradiated with the laser, and at the same time, the mice were oLiposome-coated, DOX-loaded HMNS/$SiO_2$/GQDs (HMNSs: 0.5 mg/mL, GQDs: 0.2 mg/mL, DOX: 0.3 mg/mL) were added to Eca-109 cells and irradiated with the 671-nm laser. After 20 min of irradiation, the cell viability determined by the quantitative method was only 15.23±10.61% (Figure 8B), which is in agreement with the value by the qualitative method (Figure 8A (e)).

### 3.6.3. Combination of laser irradiation and magnetic field exposure on cancer cells

Cell killing by DOX-loaded HMNS/$SiO_2$/GQDs was investigated by exposure to both laser irradiation and a magnetic field. As shown in Figure 8A(c), 8A(f), and 8B, most of the Eca-109 cells have died (viability: 16.36±4.55%) when incubated with the LP-HMNS/$SiO_2$/GQDs (HMNSs: 0.5 mg/mL, GQDs: 0.2 mg/mL), irradiated with the 671-nm laser for 20 min, and exposed to the magnetic field for 20 min. Nearly all the cells died (viability: 9.80±9.31%) when incubated with the liposome-coated DOX-loaded HMNS/$SiO_2$/GQDs (HMNSs: 0.5 mg/mL, GQDs: 0.2 mg/mL, DOX: 0.3 mg/mL), followed by 20 min of 671-nm laser irradiation and exposure to a magnetic field.

## 4. Conclusions

In summary, we successfully combined magneto mechanical, photothermal, photodynamic, and chemo therapies in a multimodal cancer therapy system using a hollow magnetic $Fe_3O_4$ nanosphere. The system was decorated with GQD and loaded with DOX (HMNS/$SiO_2$/GQDs-DOX) for photodynamic and drug release treatments. We demonstrated efficient cell killing by LP-HMNSs, activated by a magnetic field and NIR irradiation. The length of exposure to

the magnetic field was found to correlate well with the number of dead cells. NIR laser irradiation was also found to efficiently destroy cancer cells through the photothermal effect. The viability of cells treated with a combination of the mechanical and photothermal effects was significantly lower than those treated with only one stimulus. Importantly, the DOX-loaded HMNS/$SiO_2$/GQDs nanocomposites, coated with the lipid layers, exhibited the strongest effect in cell killing with magnetic field stimulation and NIR laser irradiation. These results clearly show the synergistic effects of the magneto-mechanical, photothermal, photodynamic, and chemo therapies. This unique nanocomposite system, combined with several lethal cell killing means, can simultaneously and multilaterally destroy cancer cells with a much higher efficiency.

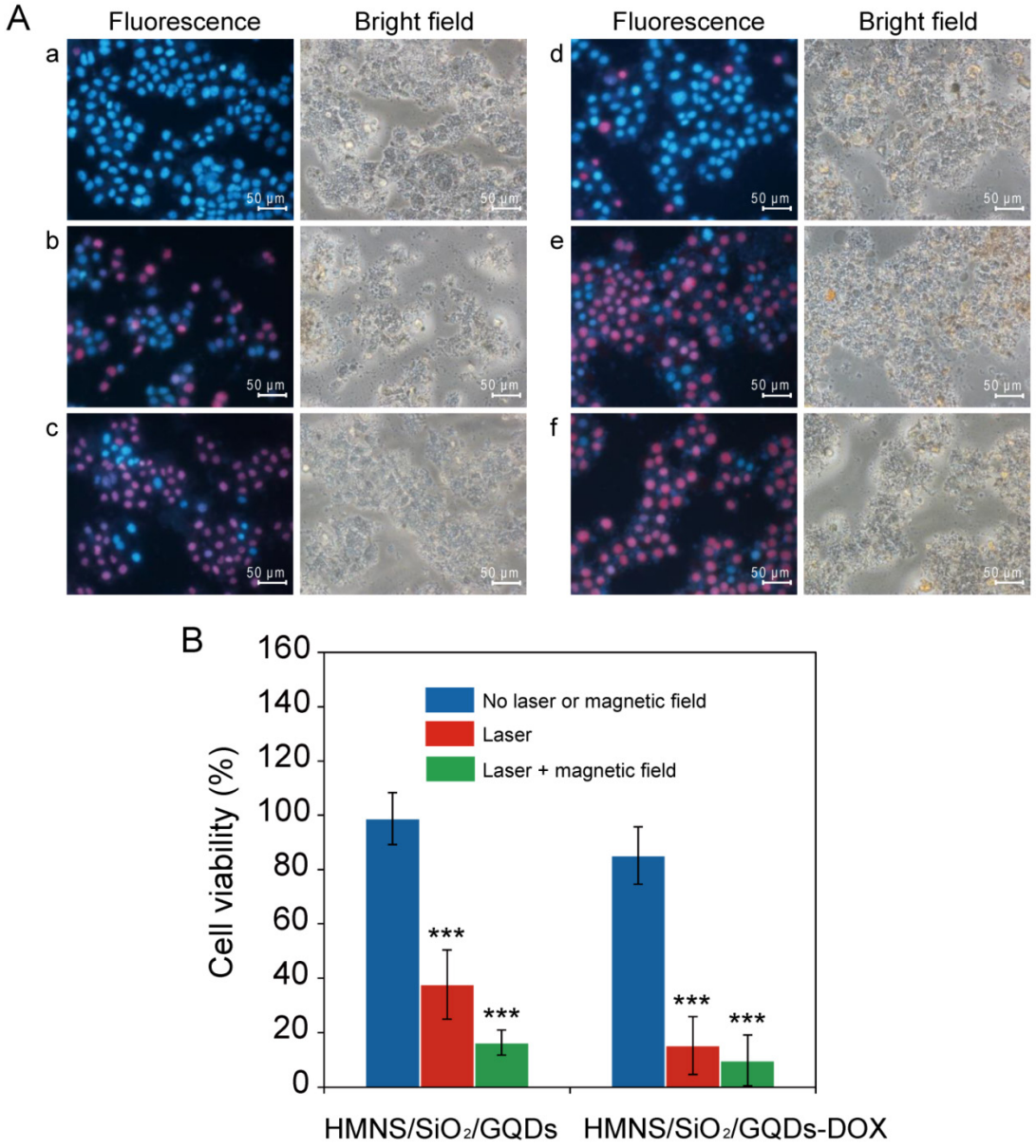


**Figure 8.** The efficacy of LP-HMNS/$SiO_2$/GQDs or LP-HMNS/$SiO_2$/GQDs-DOX for triggering Eca-109 cancer cell death induced by 671-nm laser irradiation or both 671-nm laser and magnetic field-mediated mechanical stimuli. (A) Qualitative and (B) quantitative analysis of cell viability. The Eca-109 cells were incubated with LP-HMNS/SiO2/GQDs and exposed to (a) no laser or magnetic field, (b) irradiation by a 671-nm laser for 20 min, and (c) irradiation by a 671-nm laser for 20 min followed by exposure to a magnetic field for 20 min. (d), (e), and (f) were cells incubated with LP-HMNS/$SiO_2$/GQDs-DOX for the same treatment as described in (a), (b), and (c), respectively. For the cell experiments, both HMNS/$SiO_2$/GQDs and HMNS/$SiO_2$/GQDs-DOX were coated with liposomes and dispersed in a culture medium containing PVP. The concentrations of the HMNSs, GQDs, DOX, lipids, and PVP were 0.5, 0.2, 0.3, 2.5, and 20 mg/mL, respectively. The significance level observed was *** $P<0.001$, in comparison with the group values of cells incubated with LP-HMNS/$SiO_2$/GQDs or LP-HMNS/$SiO_2$/GQDs-DOX without laser and magnetic field treatment. Data are expressed as the mean ± the standard deviation. The error bars are based on five experiments per group.

## Supplementary Material

Supplementary methods and Figure S1-S9.
http://www.thno.org/v06p0485s1.pdf

## Acknowledgements

We would like to gratefully acknowledge Prof. Qingrong Lv (School of Physics and Materials Science, Anhui University) for her assistance in the synthesis of hollow magnetic nanospheres. This work was supported in part by the National Natural Science Foundation of China (81071833, 31370961), the Nanoscience Foundation of Shanghai (13NM1402000), the Program for New Century Excellent Talents in University (NCET-07-0618).

## Competing Interests

The authors have declared that no competing interest exists.

## References

1. Thiesen B, Jordan A. clinical applications of magnetic nanoparticles for hyperthermia. Int J Hyperther. 2008; 24: 467-74.
2. Jordan A, Scholz R, Maier-Hauff K, Johannsen M, Wust P, Nadobny J, et al. Presentation of a new magnetic field therapy system for the treatment of human solid tumors with mgnetic fluid hyperthermia. J Magn Magn Mater. 2001; 225: 118-26.
3. Maier-Hauff K, Ulrich F, Nestler D, Niehoff H, Wust P, Thiesen B, et al. Efficacy and safety of intratumoral thermotherapy using magnetic iron-oxide nanoparticles combined with external beam radiotherapy on patients with recurrent glioblastoma multiforme. J Neuro-Oncol. 2011; 103: 317-24.
4. Maier-Hauff K, Rothe R, Scholz R, Gneveckow U, Wust P, Thiesen B, et al. Intracranial thermotherapy using magnetic nanoparticles combined with external beam radiotherapy: results of a feasibility study on patients with glioblastoma multiforme. J Neuro-Oncol. 2007; 81: 53-60.
5. Johannsen M, Gneueckow U, Thiesen B, Taymoorian K, Cho CH, Waldofner N, et al. Thermotherapy of prostate cancer using magnetic nanoparticles: feasibility, imaging, and three-dimensional temperature distribution. Eur Urol. 2007; 52: 1653-62.
6. Johannsen M, Gneveckow U, Taymoorian K, Thiesen B, Waldofner N, Scholz R, et al. Morbidity and quality of life during thermotherapy using magnetic nanoparticles in locally recurrent prostate cancer: results of a prospective phase I trial. Int J Hyperther. 2007; 23: 315-23.
7. Kim DH, Rozhkova EA, Ulasov IV, Bader SD, Rajh T, Lesniak MS, et al. Biofunctionalized magnetic-vortex microdiscs for targeted cancer-cell destruction. Nat Mater. 2010; 9: 165-71.
8. Domenech M, Marrero-Berrios I, Torres-Lugo M, Rinaldi C. Lysosomal membrane permeabilization by targeted magnetic nanoparticles in alternating magnetic fields. ACS nano. 2013; 7: 5091-101.
9. Zhang EM, Kircher MF, Koch M, Eliasson L, Goldberg SN, Renstrom E. Dynamic magnetic fields remote-control apoptosis via nanoparticle rotation. ACS Nano. 2014; 8: 3192-201.
10. Cheng DF, Li X, Zhang GX, Shi HC. Morphological effect of oscillating magnetic nanoparticles in killing tumor cells. Nanoscale Res Lett. 2014; 9: 195.
11. Chen HW, Burnett J, Zhang FX, Zhang JM, Paholak H, Sun DX. Highly crystallized iron oxide nanoparticles as effective and biodegradable mediators for photothermal cancer therapy. J Mater Chem B. 2014; 2: 757-65.
12. Chu MQ, Shao YX, Peng JL, Dai XY, Li HK, Wu QS, et al. Near-infrared laser light mediated cancer therapy by photothermal effect of $Fe_3O_4$ magnetic nanoparticles. Biomaterials. 2013; 34: 4078-88.
13. Shen S, Kong FF, Guo XM, Wu L, Shen HJ, Xie M, et al. CMCTS stabilized $Fe_3O_4$ particles with extremely low toxicity as highly efficient near-infrared photothermal agents for *in vivo* tumor ablation. Nanoscale. 2013; 5: 8056-66.
14. Liao MY, Lai PS, Yu HP, Lin HP, Huang CC. Innovative ligand-assisted synthesis of NIR-activated iron oxide for cancer theranostics. Chem Commun. 2012; 48: 5319-21.
15. Tian QW, Hu JQ, Zhu YH, Zou RJ, Chen ZG, Yang SP, et al. Sub-10 nm $Fe_3O_4$@$Cu_2$-xS core-shell nanoparticles for dual-modal imaging and photothermal therapy. J Am Chem Soc. 2013; 135: 8571-7.
16. Yu J, Yin WY, Zheng XP, Tian G, Zhang X, Bao T, et al. Smat $MoS_2$/$Fe_3O_4$ nanotheranostic for magnetically targeted photothermal therapy guided by magnetic resonance/photoacoustic imaging. Theranostics. 2015; 5: 931-45.
17. Gray J, Fullarton G. The current role of photodynamic therapy in oesophageal dysplasia and cancer. Photodiag Photodyn Ther. 2007; 4: 151-9.
18. Eichler J, Liebetruth J, London RA, Ziegenhagen L. Temperature distribution for combined laser hyperthermia–photodynamic therapy in the esophagus. Med Eng Phys. 2000; 22: 307-12.
19. Muijs CT, Beukema JC, Pruim J, Mul VE, Groen H, Plukker JT, et al. A systematic review on the role of FDG-PET/CT in tumour delineation and radiotherapy planning in patients with esophageal cancer. Radiother Oncol. 2010; 97: 165-71.
20. Wang XJ, Sun X, Lao J, He H, Cheng TT, Wang MQ, et al. Multifunctional graphene quantum dots for simultaneous targeted cellular imaging and drug delivery. Colloids Surf B. 2014; 122: 638-44.
21. Ge J, Lan M, Zhou B, Liu W, Guo L, Wang H, et al. A graphene quantum dot photodynamic therapy agent with high singlet oxygen generation. Nature communications. 2014; 5: 4596.
22. Chong Y, Ma YF, Shen H, Tu XL, Zhou X, Xu JY, et al. The *in vitro* and *in vivo* toxicity of graphene quantum dots. Biomaterials. 2014; 35: 5041-8.
23. Hu P, Yu LJ, Zuo AH, Guo CY, Yuan FL. Fabrication of monodisperse magnetite hollow spheres. J Phys Chem C. 2009; 113:900-6.
24. Wu X, Tian F, Wang WX, Chen J, Wu M, Zhao JX. Fabrication of highly fluorescent graphene quantum dots using L-glutamic acid for *in vitro/in vivo* imaging and sensing. J Mater Chem C. 2013; 1: 4676-84.
25. Chu MQ, Peng JL, Zhao JJ, Liang SL, Shao YX, Wu Q. Laser light triggered-activated carbon nanosystem for cancer therapy. Biomaterials. 2013; 34: 1820-32.
26. Raaphorst GP. Fundamental aspects of hyperthermic biology. In: an introduction to the practical aspects of clinical hyperthermia. Field SB, Hand JW, Eds. London: Taylor & Francis. 1990: 10-54.
27. Yu Y, Duan J, Yu Y, Li Y, Liu X, Zhou X, et al. Silica nanoparticles induce autophagy and autophagic cell death in HepG2 cells triggered by reactive oxygen species. J Hazard Mater. 2014; 270: 176-86.